

Understanding Humidity-Enhanced Adhesion of Geckos: Deep Neural Network-Assisted Multi-Scale Molecular Modeling

Tobias Materzok,* Hossein Eslami, Stanislav N. Gorb, and Florian Müller-Plathe

A higher relative humidity leads to an increased sticking power of gecko feet to surfaces. The molecular mechanism responsible for this increase, however, is not clear. Capillary forces, water mediating keratin-surface contacts and water-induced softening of the keratin are proposed as candidates. In previous work, strong evidence for water mediation is found but indirect effects via increased flexibility are not completely ruled out. This article studies the latter hypothesis by a bottom-up coarse-grained mesoscale model of an entire gecko spatula designed without explicit water particles, so that capillary action and water-mediation are excluded. The elasticity of this model is adjusted with a deep neural network to atomistic elastic constants, including water at different concentrations. Our results show clearly that on nanoscopic flat surfaces, the softening of keratin by water uptake cannot nearly account for the experimentally observed increase in gecko sticking power. Here, the dominant mechanism is the mediation of keratin-surface contacts by intervening water molecules. This mechanism remains important on nanostructured surfaces. Here, however, a water-induced increase of the keratin flexibility may enable the spatula to follow surface features smaller than itself and thereby increase the number of contacts with the surface. This leads to an appreciable but not dominant contribution to the humidity-increased adhesion. Recently, by atomistic grand-canonical molecular dynamics simulation, the room-temperature isotherm is obtained for the sorption of water into gecko keratin, to the authors' knowledge, the first such relation for any beta-keratin. In this work, it relates the equilibrium water content of the keratin to the ambient relative humidity.

sticky spatulae at the end of billions of setae on their toes form direct contact with surfaces.^[2] This direct molecular contact with the surface leads to van der Waals interactions on hydrophobic surfaces resulting in excellent adhesion.^[2] Furthermore, experimental^[3,7-9] and computational^[10,11] works show a link between relative humidity and increased adhesion. Compared to dry spatulae, humidity can enhance the stickiness by up to 300%.^[10] In experiments, the spatulae have been attached to surfaces and pulled off using atomic force microscopy (AFM), allowing only investigations of micrometer resolution. As a consequence, the humidity effect is still intensively debated.^[3,4,12,13] Some authors^[9,12-15] believe that the change in the Young modulus of gecko keratin upon swelling, so-called material softening, is responsible for the humidity-enhanced adhesion. Capillary forces induced by absorbed water on the surface are another explanation for the enhanced adhesion.^[3,7] Mitchell et al.^[9] recently inferred that the two mechanisms are not mutually exclusive: while capillary forces increase adhesion on hydrophilic surfaces, material softening increases stickiness on hydrophobic surfaces.


Recently, we have put forward a different explanation for humidity-enhanced adhesion: water fills gaps between the spatula and the surface and smoothes the spatula-surface interface.^[10] It locally increases the number density of keratin at the surface and facilitates more van der

1. Introduction

Geckos can climb vertically^[1] and even upside down on flat^[2-4] and rough^[5,6] hydrophobic and hydrophilic surfaces. Hundreds of

T. Materzok, H. Eslami, F. Müller-Plathe
Eduard-Zintl-Institut für Anorganische und Physikalische Chemie
and Profile Area Thermofluids and Interfaces
Technische Universität Darmstadt
Alarich-Weiss-Str. 8, D-64287 Darmstadt, Germany
E-mail: t.materzok@theo.chemie.tu-darmstadt.de

H. Eslami
Department of Chemistry
Colleges of Sciences
Persian Gulf University
Boushehr 75168, Iran
S. N. Gorb
Zoological Institute Functional Morphology and Biomechanics
Kiel University
Am Botanischen Garten 1-9, D-24118 Kiel, Germany

 The ORCID identification number(s) for the author(s) of this article can be found under <https://doi.org/10.1002/smll.202206085>.

© 2023 The Authors. Small published by Wiley-VCH GmbH. This is an open access article under the terms of the Creative Commons Attribution License, which permits use, distribution and reproduction in any medium, provided the original work is properly cited.

DOI: 10.1002/smll.202206085

Waals interactions with the hydrophobic surface.^[11] We call this the water mediating effect.^[10,11] Water mediating is distinctly different from capillary forces as it does not refer to a water volume but water molecules that form bridges between surface and spatula. Water molecules stick to the hydrophilic keratin protein and fill surface-spatula gaps, making the interface smoother. Water mediation is present even at low humidities and its effect on adhesion may follow a sigmoidal function, as we will discuss later. Furthermore, as the water mediation does not require an entire layer of adsorbed water as the capillary hypothesis does^[3,7,16] but on individual water molecules, this effect can explain humidity-increased adhesion even at very hydrophobic surfaces.

Complementary to experiments, molecular dynamics (MD) simulations provide detailed atomistic-level information about the system. This allows us to elucidate underlying processes during spatula pull-off. To this end, we have done coarse-grained^[10] (CG) and united-atom^[11] (UA) simulations to confirm the water mediating effect. Furthermore,^[17] we have developed a mesoscale model of a whole spatula, which reproduces pull-off pressure, Young's modulus, and Poisson's ratio of the UA keratin model. The mesoscale spatula model comprises particles (beads randomly distributed) in an actual spatula shape, acquired by scanning electron microscopy imaging of Xu et al.^[18] In the mesoscale model, each bead maps five whole keratin molecules into a single interaction site. We tuned the anisotropic bonded force field that harmonically connects each bead with at least 30 neighboring beads to yield the material properties of the dry UA keratin. We then parameterized the spatula-surface Lennard–Jones interaction to replicate the UA keratin pull-off pressure (at a specific loading rate). We have shown before that the mesoscale spatula model reproduces AFM single-spatula experimental pull-off forces^[3,5,7] (≈ 10 nN) when extrapolated to loading rates typically used in these experiments.^[17] The validation of the mesoscale spatula model is a significant new result, as no other prior work exist that reproduced experimental spatula pull-off forces in a bottom-up manner.

In the simulations explained above, the presence of water molecules may lead to material softening, capillary forces, and the water mediating effect. In the present work, we isolate the effect of water-induced material softening on the pull-off force from capillary forces and the water mediating effect. We explicitly do not simulate water molecules to investigate the effect of spatula softness without water molecules being present but set the elasticity of the keratin to the same values it would have if it contained water. In this way, we can separate the two possible mechanisms by which water leads to enhanced adhesion: 1) through mediation by water molecules (explicitly excluded

here) and 2) through a water-induced flexibility increase in the keratin (included here).

Since the relationship between water content (solubility) in spatula gecko keratin and the ambient relative humidity is experimentally not known, we previously^[19] computed it using our united-atom keratin model. Subsequently, we tune the mesoscale anisotropic force field to reproduce, without water molecules present, the reduced Young modulus, which is normally due to water-induced softening.^[12] The value of Young's modulus of water-loaded keratin, we have previously obtained in the united-atom reference model.^[11] Therefore, any change in stickiness upon adding water to keratin can be attributed to the material softening effect but not to the capillary forces and/or the water mediator effect.

We extend the mesoscale model with four additional, deep neural network-derived, bonded force fields, which implicitly model different water contents. The spatulae are linked to a virtual cantilever and pulled away from surfaces with constant velocity to mimic the AFM experiments. The mesoscale surface model was developed previously^[17] to simulate hydrophobic crystalline surfaces of tuneable roughness. We establish the first link between relative humidity, the water content in the keratin, the change in elasticity and material softening-induced adhesion.

2. Methods and Models

2.1. United-Atom Gecko Keratin Model

Our previously developed united-atom (UA) gecko keratin model is based on the GROMOS 54A7 force field.^[20–23] It is made up of an amorphous gecko beta-keratin protein (Gecprp-9), where only the intrinsically disordered parts of the protein are considered. It was assumed that only intrinsically disordered protein regions (IDRs) directly contact the surface and are responsible for the adhesive energetic interaction between spatula and surface.^[11] The water model is SPC/E.^[24] Section S2 (Supporting Information) summarizes some simulation details, which are discussed in more detail elsewhere.^[11]

Previously, we computed Young's modulus, E , and Poisson's ratio, ν , for the dry UA gecko keratin system (0 wt.% of water) and a system of wet keratin containing 10 wt.% water.^[11] Here, we simulate two additional wet keratin systems containing: 5 and 20 wt.% water, and we compute E and ν for both new water contents. **Table 1** summarizes all UA-derived E and ν .

Experimentally reported Young's moduli range from 1.2 GPa in nanoindentation tests to 7.3 ± 1.0 GPa during in situ tensile

Table 1. The calculated Young' moduli and Poisson' ratios of keratin-water mixtures at different water contents. The subscripts "UA" and "meso" refer to calculations using united-atom and mesoscale models, respectively. The water contents are connected to relative humidity (RHs) according to the results presented in **Figure 1**. Computations are performed as described in the united-atom gecko keratin work^[11] and the mesoscale work.^[17]

wt.%	RH [%]	E_{UA} [GPa]	ν_{UA}	E_{meso} [GPa]	ν_{meso}
0	0	4.53	0.409	4.529 ± 0.033	0.409 ± 0.002
5	52	4.03	0.437	4.038 ± 0.045	0.435 ± 0.002
10	86	3.84	0.423	3.838 ± 0.040	0.422 ± 0.002
20	100	2.28	0.475	2.247 ± 0.025	0.496 ± 0.004

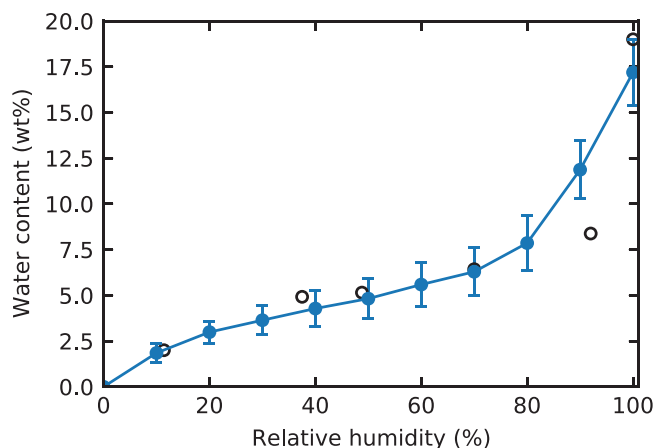


Figure 1. Water content of gecko keratin, as a function of relative humidity, calculated using our united-atom gecko keratin model.^[11] The filled (blue) and open (black) markers are the results of the grand canonical ensemble simulations^[19] and experimental data for the dorsal and ventral scales of the snake *Naja nigricollis*, respectively, and the curve connects the calculated points. Error bars are the root-mean-square deviation of concentration of water in keratin from the average value.

tests.^[14] Humidity affects the elasticity of setal keratin, as 30% relative humidity yields $E = 3.2 \pm 0.2$ GPa and with increased humidity of 80% Young's modulus decreases to 2.2 ± 0.2 GPa.^[12] In a computational model, previously developed in our group, dry seta keratin was found to be rather stiff with $E = 9.2$ GPa.^[25] The Young moduli of the UA dry and wet spatulae are, therefore, within the range of experimental values.

2.2. Water Solubility in Gecko Keratin

The details of the calculation of water solubility in gecko keratin, as a function of RH, are reported elsewhere.^[19] Here, we only report a summary, which is needed to understand the essential elements of the method. We performed MD simulations in the grand canonical ensemble (GCE) to find the phase coexistence point (vapor pressure of water and equilibrium density of water in the keratin phase) at 300 K. In the GCE simulation method,^[26] the system (keratin plus water) couples to an ideal gas reservoir of water molecules through a coupling parameter. A fractional molecule, whose potential energy of interaction with the rest of the system is scaled with the coupling parameter, is added to the system, and the equation of motion for the coupling parameter is solved. The coupling parameter varies dynamically between 0 and 1; when it reaches 0, a water molecule is removed from the system. When it reaches 1, the fractional water molecule becomes a fully coupled molecule. In equilibrium, the number of water molecules in the keratin phase fluctuates around an average value, consistent with the imposed conditions (fixed chemical potential, temperature, and volume). Because adhesion and gecko keratin softening by water uptake depends on the water content inside keratin and its relation with the RH, we reproduce our calculated sorption isotherm of water in gecko keratin^[19] in Figure 1. We have also shown in Figure 1 our experimental data on the water uptake of dorsal and ventral scales of the snake *Naja*

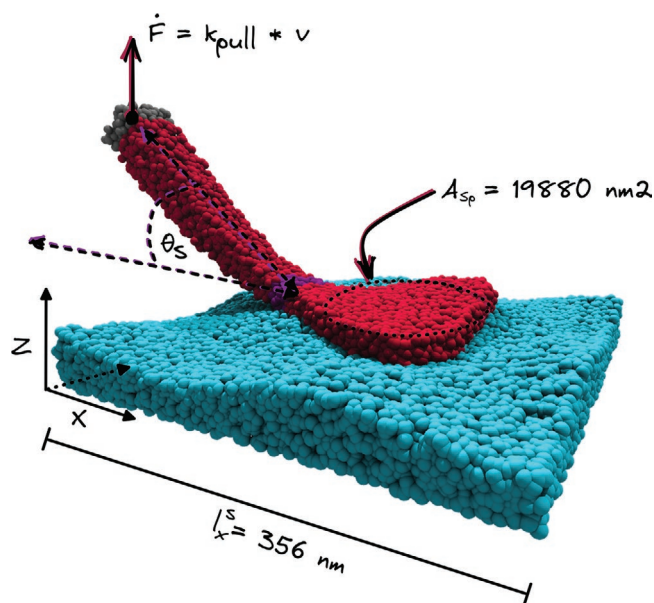


Figure 2. Snapshot of the mesoscale spatula (red) on a rough hydrophobic surface (cyan). During pull-off simulations, a virtual cantilever is linked to the shaft haft and pulled vertically with loading rate \dot{F} , to mimic atomic force microscopy experiments, as we discuss in Section 2.6.

nigricollis and the claw tips of the Tokay gecko (*Gekko Gecko*) toes (≈ 30 g water/100 g sample at 100% RH) at 297 K and 100% RH. The calculated sorption isotherm has a general sigmoidal shape, consistent with that for water sorption in α -keratin.^[27,28]

2.3. Mesoscale Spatula Model

The spatula model (Figure 2) uses the previously derived mesoscale keratin force field^[17] that was validated against experimental single-spatula AFM experiments with typical pull-off forces in the range of 8–20 nN^[3,5,7] when used with an actual spatula shape. The experimental setup used in AFM studies to investigate single-spatula pull-off forces is shown in Figure S1 (Supporting Information). The elastic and structural properties of the spatula are modeled with a simple bead spring model with directional force constants to mimic the fibrillar structure present in gecko spatulae.^[10,11,17,25,29–31]

The beta-sheet region (Core-box region^[30,31]) of the Ge-cprp-9 peptide (which, in the united-atom simulation of keratin, was omitted, see Section 2.1) forms dimers. The dimers polymerize into nanofibrils,^[32] which associate to mesoscale fibrils.^[25,29,30] These fibrils are visible in scanning electron microscopy (SEM) cross sections of gecko setae, and the spatula is possibly made up of almost pure fibrils.^[29] The fibrils significantly contribute to the mechanical properties of gecko spatulae. Consequently, the model must describe the anisotropic elasticity arising from fibrils inside the spatula. Since the spatula model consists of randomly distributed, highly coarse-grained beads that each incorporate the mass of about five keratin proteins, we have to model the fibrils implicitly.^[17] The bead-bead harmonic bond potential is expressed as $V(r) = K/2 \cdot (r - b_0)^2$, b_0 and K being the equilibrium bond length and the force constant,

respectively. For each bond, these parameters are unique. Once assigned, all K and b_0 stay unchanged. The value of K increases, as the initial direction of a bond aligns with the direction of the “virtual” fibril:

$$K = k + k_b \cdot |\cos \theta| \quad (1)$$

where k and k_b are the isotropic part of the force constant and the force constant in the fibril direction, respectively, and θ is the angle between the bond vector and the “virtual” fibril direction. Hence, the spatula model implicitly accounts for fibrils due to the anisotropy of the bonded potential. The potential is adjusted such that in equilibrium, the spatula shaft is bent by $\theta_s = 45$ degrees with respect to the surface (Figure 2). The effect of pre-bent spatulae on the adhesion is discussed elsewhere.^[17]

A Lennard–Jones (12–6) potential models the adhesive interactions with the surface, as is discussed in more detail in the previous work.^[17] The spatula-surface interaction was parameterized against the pull-off pressure (pull-off force normalized by the area) of the dry UA gecko keratin model.^[11]

The mesoscale keratin model was optimized against the material properties of the dry UA gecko keratin model in our previous work.^[17] We here extend the mesoscale spatula model and optimize k and k_b against properties of wet keratin at different implicit relative humidities using a deep neural network (see Section 2.5). We do not change the spatula-surface interaction, and the mesoscale model does not include water particles. As a result, any changes in stickiness are uniquely due to the changed elastic material properties. This allows us to isolate the effect of keratin softening from capillary forces and the water mediating effect.^[10,11]

2.4. Mesoscale Surface Models

The mesoscale spatula is attached to and detached from hydrophobic surfaces (water contact angle $\theta_c \approx 110^\circ$) of varying roughnesses which are modeled by a particle model of similar beads size.^[11,17] The surface follows a two-dimensional sinusoidal topography and has the same density as the spatula material. The minimum thickness z_m of the slab representing the surface is always 24 nm. The 3D landscape is defined by $z_m = 24 \text{ nm} + 8 \text{ nm} \cdot \sin(x \cdot \pi n_p / l_x^s + \pi X_x) \cdot \sin(y \cdot \pi n_p / l_y^s + \pi X_y)$, where 8 nm is the peak height, n_p is the number of peaks in the x- and y-direction, and l_x^s and l_y^s are the lengths of the surface in the x- and y-directions, respectively.

To simulate random placements of the spatula on top of a surface (see Figure 3), we apply a random phase shift using a uniformly distributed random number $X \sim U([0, 2])$ in the x and y directions. We generate eight surfaces with peak densities ρ_p ranging from $\rho_p = 0$ to $394.12 \mu\text{m}^{-2}$. The surface has an area of $356 \text{ nm} \times 356 \text{ nm}$.

We expect a surface describing an oxide mineral (e.g., the amorphous silica substrate of Huber et al. used in the UA model) not to be deformable. Such a surface is orders of magnitude stiffer than gecko keratin. Thus, we choose to make our surface entirely rigid. Therefore, surface beads are frozen and only interact with the keratin. As a result, the surface acts as a space-fixed attractive 3D external potential.

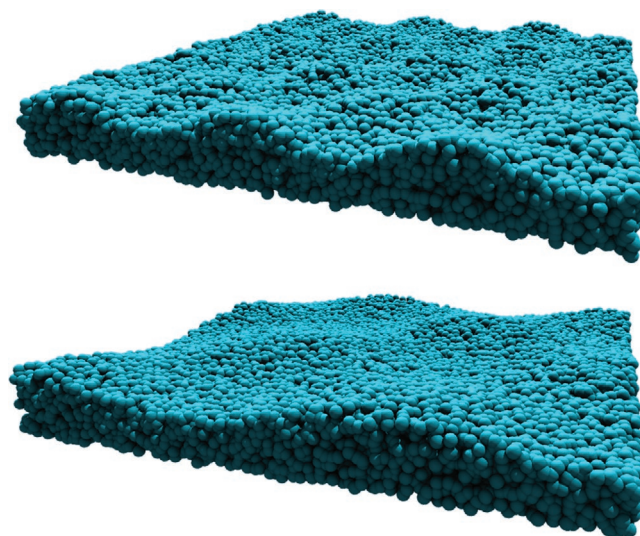


Figure 3. Two surfaces with different peak densities (top $\rho_p = 141.88 \mu\text{m}^{-2}$ and bottom $\rho_p = 39.41 \mu\text{m}^{-2}$). The center of the surface (where the spatula attaches), can present anything between a valley and a peak, depending on phase shift. The height between the peak and valley (amplitude) is 16 nm for all surfaces, resulting in a root-mean-squared roughness of 4 nm.

2.5. Parameterizing the Mesoscale Spatula Model with Implicit Water Contents

The “wet” mesoscale spatula model should explicitly only reproduce the change in material properties due to water-induced material softening. We, thus, optimize only the isotropic part, k , and the anisotropic part, k_b , of the bond force constant K (Section 2.3) against the elastic properties of wet keratin as determined from united-atom simulations (Section 2.1). We create four bonded force fields that reproduce Young’s modulus and Poisson’s ratio at 0, 5, 10, and 20 wt.% water contents.

We use existing parameter-exploration simulations of the previous work^[17] to train a deep neural network (DNN). Grid search-based hyperparameter tuning yields a network architecture that does not overfit. The DNN feeds the input vector (of the two scalars) k and k_b to a fully connected layer (6x64) and subsequently an output layer (1x2). The output layer maps to Young’s modulus E and Poisson’s ratio ν of the mesoscale keratin. The DNN generalizes the regression between the inputs and the outputs well and performs better in the prediction of E than a bilinear fit of E against the scalars k and k_b . In Section S1 (Supporting Information), a detailed description of the DNN can be found (source code and DNN weights are available at github.com/TobiasMaterzok/DNN-Gecko-Implicit-Water).

We use the DNN to predict the force constant coefficients k and k_b corresponding to the material properties of wet keratin (computed using the united-atom keratin model, Section 2.1) to model the water content in the mesoscale spatula implicitly. Figure 4 shows the DNN-interpolated solution landscape. Black dots represent actual simulations performed during the previously discussed parameter exploration.

The DNN derived anisotropic force constant coefficients (summarized in Table S1, Supporting Information) are validated by stress-strain simulations (details in Section S2, Supporting Information). Strains of 0%, 1%, and 2% are applied in the

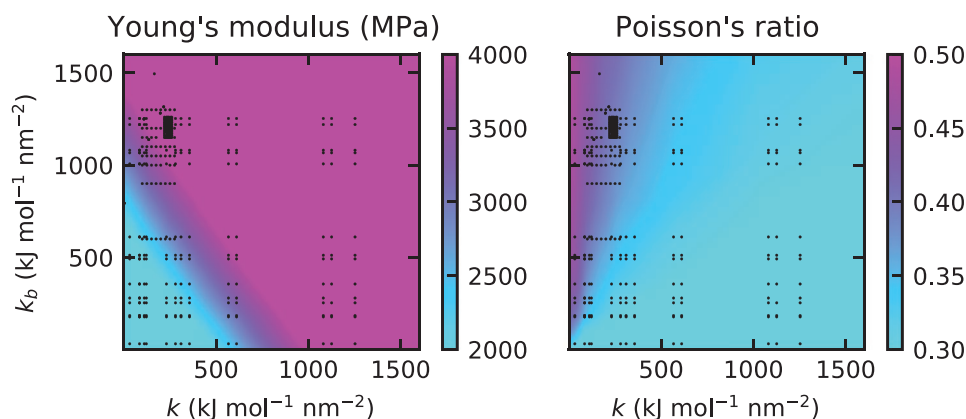


Figure 4. Result of the deep neural network prediction of Young's modulus E and Poisson's ratio ν from the force constant coefficients k and k_b . Black dots are actual simulations done previously,^[17] during our parameterization of the dry spatula model. The black dots are denser in the upper left corner as we have tuned the search space to find the values corresponding to $E = 4.5$ GPa and $\nu = 0.4$ of corresponding to dry gecko keratin.

(virtual) fibril direction for ten independently created keratin systems for each coefficient combination (4×10 simulations in total) to compute E and ν . The method is described in our previous work.^[17]

As a result, we can relate Young's modulus and Poisson's ratio of the UA keratin (Section 2.1) and mesoscale spatula model (this section) to the water content (and relative humidity) (Section 2.2), as summarized in Table 1.

2.6. Spatula Detachment Simulations

Gecko spatulae attached to surfaces can be inclined (inclination angle θ_s , Figure 2), and in experimental imaging, a whole range of possible inclinations have been observed.^[33,34] In previous work,^[17] we tested $\theta_s = 45^\circ$ to $\theta_s = 75^\circ$ and found a direct relationship between the pull-off force and θ_s . The smallest pull-off force was found for $\theta_s = 45^\circ$, and it also had the smallest standard deviation.

We use the bent equilibrium configurations of spatulae of the previous work (with an inclination of $\theta_s = 45^\circ$) to perform non-equilibrium pulling simulations.^[17]

A preload is applied for 600 ns to initially attach the spatula to the surface. In this preload step, an external pressure of 0.4 pN nm⁻² presses the spatula pad against the surface, as was done in the experiment by Xu et al.^[18] After the preload, the system is allowed to relax for 500 ns without any external force. These simulation times are sufficient to converge the distance between spatulae and surfaces.

In the pull-off simulations, the attached spatulae are pulled away from the surfaces by linking the center of mass of the spatula shaft haft (Figure 2) to a virtual cantilever. The link is modeled by a harmonic potential with a force constant of $k_{\text{pull}} = 1000$ kJ mol⁻¹ nm⁻². The virtual cantilever is moved at a constant pulling velocity vertically away from the surface. The harmonic potential of the linker and the pulling velocity results in a theoretical^[35] loading rate of 1.66×10^{12} pN s⁻¹. At the pull-off force, which is the maximum in the force-displacement (or force-time) curve, the spatula detaches from the surface.

A vacuum surrounds the surface and the spatula. All spatula detachment simulations are performed in the NVT ensemble

with a thermostat keeping the temperature of the spatula constant at 300 K. The preload step uses a stochastic dynamics (SD) thermostat^[36] with $\tau_T = 1$ ps; the relaxation step uses SD with $\tau_T = 10$ ps; and all other steps use a velocity rescaling thermostat^[37] with $\tau_T = 1$ ps, following our established protocol.^[17]

3. Results and Discussion

3.1. High Relative Humidity (100%) Allows Spatulae to Stick to a Wider Range of Surface Roughness

The pull-off force (also called critical force or rupture force) is the force needed to detach the spatula from the surface and can be interpreted as the stickiness of the spatula. A detailed explanation of the spatula peel-off, including force-displacement curves, can be found in our previous work using the mesoscale spatula.^[17] Here, we are only interested in how stickiness or pull-off force depends on water-induced material softening.

The spatula area is $A_{Sp} = 19880$ nm². For illustrative purposes, the spatula pad can be viewed as an isosceles triangle of area $A_t = 19880$ nm² corresponding roughly to $A_t \approx 1/2 \times (185 \pm 10 \text{ nm}) \times (215 \pm 10 \text{ nm})$. Furthermore, we call the inverse of the peak density the peak area or valley area $A_p = A_{\text{valley}} = 1/\rho_p$. We use the ratio A_{valley}/A_{Sp} to express if the sinusoidal surface wavelength ($\pi n_p/l_s^2$) is smaller than the pad dimensions. Thus, at $A_{\text{valley}}/A_{Sp} = 1$, a valley of the sinusoidal surface topography has the same area as the spatula pad. Recall that the surface amplitude is 16 nm (Section 3.1). Figure 3 (bottom) corresponds to a ratio of $A_{\text{valley}}/A_{Sp} = 1.28$ and (bottom) $A_{\text{valley}}/A_{Sp} = 0.35$.

We computed the average pull-off force from detachment simulations of 10 independently generated spatulae and surfaces as a function of surface roughness. Figure 5A shows the pull-off force against the ratio A_{valley}/A_{Sp} . Figure S3 (Supporting Information) shows four examples of force-displacement curves; only the maximum force (the pull-off force) is used in this investigation. Finally, Figure 6 illustrates the ratio.

In agreement with our previous findings,^[17] the stickiness of the spatula as a function of the ratio A_{valley}/A_{Sp} is well described by a sigmoidal (Richards^[38]) curve (solid lines in Figure 5A) at all implicit water contents (relative humidities).

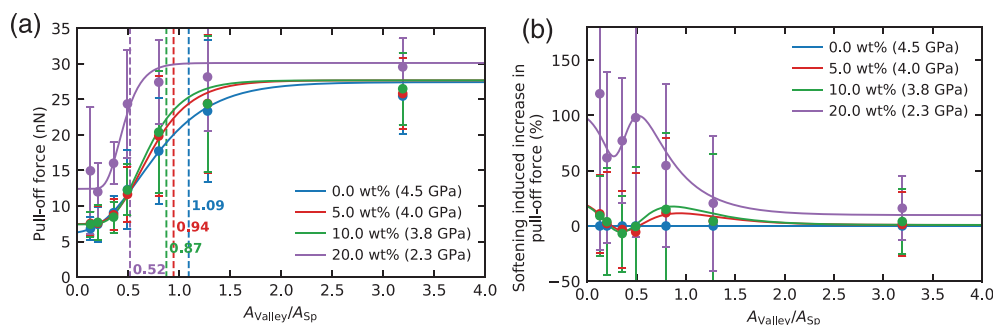


Figure 5. A) Pull-off force as a function of keratin water content and $A_{\text{valley}}/A_{\text{Sp}}$. The water content and corresponding Young's modulus are denoted in the legend. The average pull-off forces follow a sigmoidal (Richards^[38]) curve (solid lines). Vertical dashed lines denote a threshold of 80% pull-off force relative to the maximum on a flat surface. The average is computed from $n = 10$ independent samples, and the standard deviation of the mean is used as the error. B) The relative increase in pull-off force due to the implicit water content, compared to the dry spatula (blue line at 100%). The solid lines are used to guide the eye. The error is calculated as the Gaussian error propagation of the standard deviations of the mean of (A).

When $A_{\text{valley}}/A_{\text{Sp}}$ falls below a certain threshold, the spatula loses its ability to follow the surface contour, i.e., the stickiness decreases significantly. We have indicated the ratio where the stickiness falls below 80% of that of a flat surface with vertical dashed lines in Figure 5. For dry spatulae, this threshold already occurs at $A_{\text{valley}}/A_{\text{Sp}} = 1.09$. Thus, when the spatula pad area is on the same length scale as the area of surface asperities, its stickiness is 20 % lower than on an ideally flat surface.

With increasing relative humidity (higher water content, softer keratin, cf. Table 1), this threshold is only reached at smaller surface-feature sizes A_{valley} ; gecko spatulae in high relative humidity can adapt to finer surface topographies. The threshold decreases linearly with both water content and Young's modulus from 1.09 to 0.52 (Figure 5A bottom).

3.2. Non-Linear Increase in Stickiness Due to Material Softening

We also study the increase in stickiness due to humidity in percent over the dry keratin (Figure 5B). It is shown as a function of the ratio $A_{\text{valley}}/A_{\text{Sp}}$.

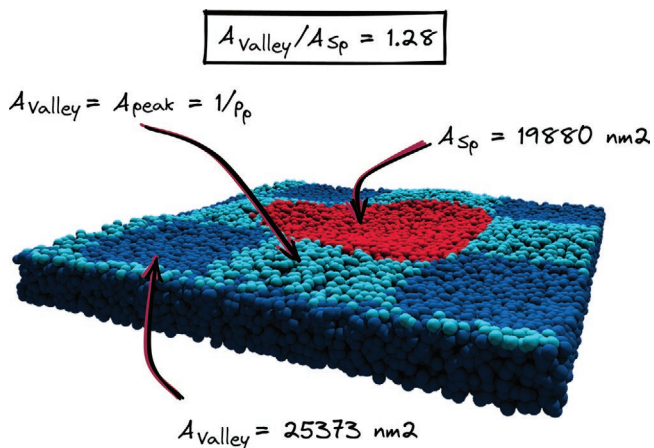


Figure 6. An illustration of the ratio of valley area against spatula pad area for the example of $A_{\text{valley}}/A_{\text{Sp}} = 1.28$. The surface peaks are cyan, and the surface valleys are blue. We color all surface beads within the cutoff length of the spatula red as an approximation to the spatula pad area. Thus, the actual spatula pad is smaller than illustrated.

On flat surfaces, there is essentially no increase of stickiness due to (implicit) humidity. This holds at all humidities (Figure 7B blue). Experimental work shows that between 1.5% and 45% relative humidity,^[3] the pull-off force increases by 60% on a flat hydrophobic surface and between 55% and 80% relative humidity,^[9] the shear adhesion increases by $158 \pm 40\%$. In contrast, our softened spatula sticks just 10% better at maximum humidity. Thus, given that the humidity-enhanced adhesion increase on flat surfaces is $\approx 200\text{--}300\%$ ^[3,9–11] in total, it follows that the material softening hypothesis can be ruled out for flat hydrophobic surfaces, as we previously conjectured from CG^[10] simulations of gecko keratin.

We, therefore, have to conclude that other mechanisms than keratin-softening are responsible for the larger stickiness at higher humidities. Based on united-atom and coarse-grained molecular dynamics, we have previously suggested that water molecules mediate the attraction between keratin and surface.^[11] The molecular-level simulations have shown that water fills the spatula-surface gaps and increases the number of interacting sites and the magnitude of interactions between surface and spatula. Since the availability of water molecules in the keratin increases sigmoidally with relative humidity (Figure 1), we expect the water mediating effect to scale similarly.

The situation is different for nanostructured surfaces. Here, the effect of material softening becomes more pronounced. Figure 7 shows a marked increase in relative stickiness at a material softness corresponding to a high (>86%) humidity or 20% water content. However, at a relative humidity below 86%, the material softening effect does not strongly influence the humidity-enhanced adhesion, even on rough surfaces. The better adhesion of wet keratin to rough surfaces is, in part, brought about by its increased flexibility and its better ability to follow small surface features (see Figures S4 and S5, Supporting Information). The effect is small at 5%, and 10% water content and only takes off at 20% water content. This is simply a consequence of the fact that the elastic modulus only becomes markedly smaller at the highest water load (Figure 7C, Table 1). However, even on rough surfaces, the moisture-induced keratin softness can only explain some fraction of the observed increase in stickiness (it is 1/3–1/2 even when compared to experimental work using single spatulae on flat surfaces^[3,9]).

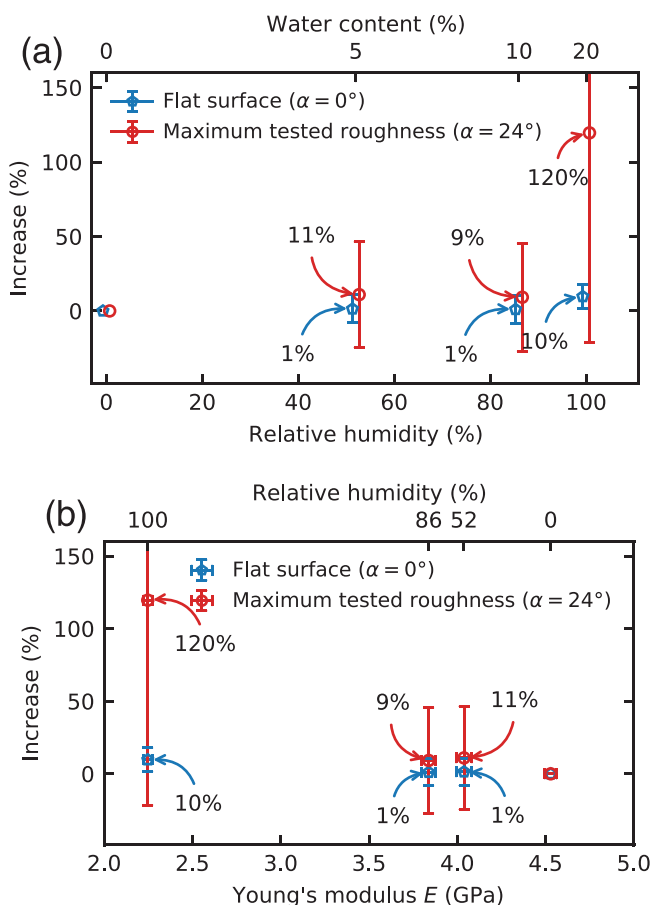


Figure 7. A) The percentage increase in the pull-off force (stickiness) of gecko spatulae due to material softening on flat and rough surfaces, compared to dry spatulae $[F(\text{RH}) - F(\text{RH} = 0\%)]/F(\text{RH} = 0\%)$. The increased pull-off force depends non-linear on implicit water content (relative humidity). The error is calculated as the Gaussian error propagation of the standard deviations from $n = 10$ independent samples. The values are offset by 0.7% relative humidity against each other to clearly show the error bars. B) The percentage increase in the pull-off force (stickiness) of gecko spatulae due to material softening on flat and rough surfaces, compared to dry spatulae. The increased pull-off force is shown as a function of Young's modulus. The error is calculated as the Gaussian error propagation of the standard deviations from $n = 10$ independent samples.

4. Conclusion

It is known that a humidity increase in the environment enhances the sticking power of geckos. Several mechanisms have been put forward to explain this feature. Most prominent are i) capillary forces, ii) water molecules mediating between surface and keratin and iii) water uptake leading to a softening of keratin (lower elastic modulus) and, consequently, stronger adhesion. We have previously reproduced the positive effect of humidity on stickiness by united-atom (UA) and coarse-grained (CG) molecular simulations. We collected strong arguments for water mediation (ii) in our simulations.^[10,11] Since we used explicit water molecules in those simulations, however, we could not rule out the indirect action of water via keratin softening (iii), which is still a very popular hypothesis in gecko biophysics.^[9,12–14] In order to separate the different mechanisms, we adapted a mesoscale

model^[17] for entire spatulae to reproduce the elasticity of water-swollen keratin without containing explicit water molecules. Thus, capillary force (i) and water-mediation (ii) are excluded from the model. The elastic constants of water-swollen keratin, in turn, were determined by atomistic simulations, and the equilibrium water content at a given relative humidity was calculated previously^[19] by atomistic grand-canonical molecular dynamics. We, thus, pursue a true multi-scale simulation protocol.

We trained a deep neural network to predict the mechanical properties, Young's modulus and Poisson's ratio, from bonded force field parameters of our previously published mesoscale spatula model reusing existing data.^[17] The trained DNN (Section 2.5) allowed us to directly infer bonded force field parameters (Section 2.3) that produce the exact target material properties instead of relying on lengthy and costly classical parameter optimization. We computed material properties for four different water contents using our united-atom (UA) gecko keratin model^[11] (Section 2.1). The DNN prediction was then used to find the necessary force field parameters of the mesoscale model to reproduce the elastic constants from the UA simulations of the water-swollen keratin. This adaptation of the mesoscale force field parameters only affects the elasticity of the keratin, not its interaction with the surface. Thus, capillary forces (i) and water-mediation (ii) cannot operate through effective interactions either. In the absence of water molecules, capillary forces and the water mediating effect can be rigorously ruled out in any observations we made.

Our results disprove the hypothesis of material softening being responsible for humidity-enhanced adhesion of spatulae on flat hydrophobic surfaces.^[3,7,9] On flat surfaces, an implicitly fully “water-soaked” keratin sticks better to a surface than complete water-free keratin by a mere 10% (Figure 7). In comparison, experimental^[3,9] and computational^[10,11] reports show that the adhesion increase due to humidity is ≈ 200 – 300% . As a result, we rule out softening as a mechanism dominating the humidity-enhanced adhesion of whole spatulae on flat surfaces. The primary mechanism underlying humidity-enhanced adhesion is the mediation of keratin-surface interactions by water. Our previous findings for wet UA gecko keratin^[11] showed that elastic interactions are one of the smaller contributions controlling the pull-off force from the flat hydrophobic surface. As an interesting side note, elasticity significantly contributes to the pull-off of dry keratin from a hydrophobic surface. However, as keratin gets wet, water mediation (ii) becomes dominant.

While material softening does not determine spatula stickiness at ideal flat surfaces, it is one critical factor at nanoscopic rough surfaces. Here, the mesoscale spatula model showed a material softening-induced increase in adhesion of up to 120% compared to dry keratin. The higher flexibility of keratin (which only becomes appreciable at water contents at or near saturation) enables the spatula to follow surface structures smaller than itself. Thus, the spatula can keep the full adhesion potential when surfaces get rougher (Section 3.1) and surface structures are smaller than the spatula.

Of the mechanisms underlying humidity, the water mediating effect dominates in all circumstances at the very hydrophobic surface except in extremely humid environments (relative humidity $>86\%$). Here, if the surface is rough and surface features are smaller than the spatula, the material softening effect may be responsible for 1/3–1/2 of the increased stickiness

compared to the dry keratin. In short, the water-induced increase in flexibility allows spatulae to follow surface features smaller than themselves, thereby increasing contact area with the surface and, thus, contributing to humidity-enhanced adhesion. In contrast, in laboratory experiments using very hydrophobic nanoscopic flat surfaces, the humidity-enhanced adhesion is determined by the water mediating effect we proposed.^[10,11] Capillary forces depend on a water volume absorbed to the surface. Capillary bridges are either completely absent on very hydrophobic surfaces at relative humidities smaller than the supersaturation limit or of convex geometry.^[10] The latter case could even lead to capillary forces that are repulsive.^[39,40]

Finally, let us discuss the generality of our findings. Here, we investigated material softening in terms of the more common single-spatula experiments; however, how does this transfer to whole setae adhesion? For the per-spatula level, we have shown the effect of material softening in this work. However, setae break up large contact areas into multiple smaller sub-areas (spatulae). This strategy is called contact splitting.^[33,41,42] Consequently, the characteristic adhesive feature length increases from the spatula's contact area to the setae's theoretical contact area. Water-softened setae, therefore, likely exhibit increased stickiness even if surface features are larger than the spatula, as long as the surface features are in the order of the theoretical seta contact area. The quantitative impact of material softening on seta-level adhesion is up for future investigation. While neither rough surfaces nor seta adhesion investigations are currently common or even well enough defined, systematic fine-grained classification of surfaces in geckos' habitats are completely absent from the literature, and seta investigations do not report the number of spatulae of the investigated setae—it will be nonetheless important to fully understand the complete adhesion strategy employed by geckos in their natural habit. Furthermore, what happens on surfaces other than the one we investigated? We have only explored a hydrophobic surface in this work. On a hydrophilic surface, water mediation is enhanced,^[11] and capillary action may become relevant at very high humidity as water can pool up. Finally, and most interesting to synthetic gecko adhesive research,^[43–49] can the results be generalized to other materials? Both this work and our first coarse-grained work^[10] use molecular models that are more generic than our more precise united-atom model.^[11] Therefore, results are generalizable to other materials with similar properties. Synthetic adhesives can create better contact if they are flexible enough to follow nanostructured surfaces. A water mediation-like effect may also be constructed with small diffusive molecules instead of water (i.e., tackifiers^[50–53]).

In this simulation study, we “deactivated” the effects of water mediation (ii) and capillary forces (i) to only investigate spatula softness (iii). In reality, spatulae are softened by water molecules, which also operate as mediators for water-surface interactions. Possible non-additive effects between the three mechanisms should be the subject of further investigation.

Supporting Information

Supporting Information is available from the Wiley Online Library or from the author.

Acknowledgements

Open access funding enabled and organized by Projekt DEAL.

Conflict of Interest

The authors declare no conflict of interest.

Data Availability Statement

The data that support the findings of this study are available from the corresponding author upon reasonable request.

Keywords

deep neural networks, gecko adhesion, humidity, molecular dynamics, multiscale molecular model, pull-off, spatula

Received: October 4, 2022

Revised: December 6, 2022

Published online: January 27, 2023

- [1] Q. Jiang, Z. Wang, J. Zhou, W. Chen, Z. Dai, *J. Bionic Eng.* **2019**, *16*, 115.
- [2] K. Autumn, Y. A. Liang, S. T. Hsieh, W. Zesch, W. P. Chan, T. W. Kenny, R. Fearing, R. J. Full, *Nature* **2000**, *405*, 681.
- [3] G. Huber, H. Mantz, R. Spolenak, K. Mecke, K. Jacobs, S. N. Gorb, E. Arzt, *Proc. Natl. Acad. Sci. U.S.A.* **2005**, *102*, 16293.
- [4] A. Y. Stark, S. Subarajan, D. Jain, P. H. Niewiarowski, A. Dhinojwala, *Philos. Trans. Royal Soc.* **2016**, *374*, 20160184.
- [5] G. Huber, S. N. Gorb, N. Hosoda, R. Spolenak, E. Arzt, *Acta Biomater.* **2007**, *3*, 607.
- [6] T. W. Kim, B. Bhushan, *Ultramicroscopy* **2007**, *107*, 902.
- [7] W. Sun, P. Neuzil, T. S. Kustandi, S. Oh, V. D. Samper, *Biophys. J.* **2005**, *89*, L14.
- [8] A. Y. Stark, M. R. Klittich, M. Sitti, P. H. Niewiarowski, A. Dhinojwala, *Sci. Rep.* **2016**, *6*, 30936.
- [9] C. T. Mitchell, C. B. Dayan, D.-M. Drotlef, M. Sitti, A. Y. Stark, *Sci. Rep.* **2020**, *10*, 19748.
- [10] T. Materzok, S. N. Gorb, F. Müller-Plathe, *Soft Matter* **2022**, *18*, 1247.
- [11] T. Materzok, A. Canestraight, S. N. Gorb, F. Müller-Plathe, *ACS Nano* **2022**, *16*, 19261.
- [12] M. Prowse, M. Wilkinson, J. Puthoff, G. Mayer, K. Autumn, *Acta Biomater.* **2010**, *7*, 733.
- [13] J. B. Puthoff, M. S. Prowse, M. Wilkinson, K. Autumn, *J. Exp. Biol.* **2010**, *213*, 3699.
- [14] G. Huber, S. Orso, R. Spolenak, U. G. K. Wegst, S. Enders, S. N. Gorb, E. Arzt, *Mater. Res.* **2008**, *99*, 1113.
- [15] D. Tan, A. Luo, X. Wang, Z. Shi, Y. Lei, M. Steinhart, A. Kovalev, S. N. Gorb, K. T. Turner, L. Xue, *ACS Appl. Nano Mater.* **2020**, *3*, 3596.
- [16] J. O. Wolff, S. N. Gorb, *Proc. Biol. Sci.* **2012**, *279*, 139.
- [17] T. Materzok, D. De Boer, S. N. Gorb, F. Müller-Plathe, *Small* **2022**, *18*, 2201674.
- [18] Q. Xu, Y. Wan, T. S. Hu, T. X. Liu, D. Tao, P. H. Niewiarowski, Y. Tian, Y. Liu, L. Dai, Y. Yang, Z. Xia, *Nat. Commun.* **2015**, *6*, 8949.
- [19] M. Khani, T. Materzok, H. Eslami, S. Gorb, F. Müller-Plathe, *J. R. Soc. Interface* **2022**, *19*, 20220372.
- [20] L. D. Schuler, X. Daura, W. F. v. Gunsteren, *J. Comput. Chem.* **2001**, *22*, 1205.

- [21] C. Oostenbrink, A. Villa, A. E. Mark, W. F. V. Gunsteren, *J. Comput. Chem.* **2004**, *25*, 1656.
- [22] N. Schmid, A. P. Eichenberger, A. Choutko, S. Riniker, M. Winger, A. E. Mark, W. F. van Gunsteren, *Eur. Biophys. J.* **2011**, *40*, 843.
- [23] W. Huang, Z. Lin, W. F. van Gunsteren, *J. Chem. Theory Comput.* **2011**, *7*, 1237.
- [24] H. J. C. Berendsen, J. R. Grigera, T. P. Straatsma, *J. Phys. Chem.* **1987**, *91*, 6269.
- [25] K. S. Endoh, T. Kawakatsu, F. Müller-Plathe, *J. Phys. Chem. B* **2018**, *122*, 2203.
- [26] H. Eslami, F. Müller-Plathe, *J. Comput. Chem.* **2007**, *28*, 1763.
- [27] S. Rosenbaum, *J. Polym. Sci.* **1970**, *31*, 45.
- [28] J. D. Leeder, I. C. Watt, *J. Phys. Chem.* **1965**, *69*, 3280.
- [29] N. W. Rizzo, K. H. Gardner, D. J. Walls, N. M. Keiper-Hrynko, T. S. Ganzke, D. L. Hallahan, *J. R. Soc. Interface* **2006**, *3*, 441.
- [30] D. L. Hallahan, N. M. Keiper-Hrynko, T. Q. Shang, T. S. Ganzke, M. Toni, L. D. Valle, L. Alibardi, *J. Exp. Zool. B: Mol. Dev. Evol.* **2009**, *312B*, 58.
- [31] L. Alibardi, *Tissue Cell* **2013**, *45*, 231.
- [32] M. Calvaresi, L. Eckhart, L. Alibardi, *J. Struct. Biol.* **2016**, *194*, 282.
- [33] E. Arzt, S. Gorb, R. Spolenak, *Proc. Natl. Acad. Sci. U.S.A.* **2003**, *100*, 10603.
- [34] G. Huber, S. N. Gorb, R. Spolenak, E. Arzt, *Biol. Lett.* **2005**, *1*, 2.
- [35] H. Grubmüller, *Methods Mol. Biol.* **2005**, *305*, 493.
- [36] N. Goga, A. J. Rzepiela, A. H. de Vries, S. J. Marrink, H. J. C. Berendsen, *J. Chem. Theory Comput.* **2012**, *8*, 3637.
- [37] G. Bussi, D. Donadio, M. Parrinello, *J. Chem. Phys.* **2007**, *126*, 014101.
- [38] F. J. Richards, *J. Exp. Bot.* **1959**, *10*, 290.
- [39] M. Dörmann, H.-J. Schmid, *Procedia Eng.* **2015**, *102*, 14.
- [40] P. A. Kralchevsky, K. Nagayama, in *Particles at Fluids Interfaces and Membranes*, 1st ed., (Eds.: P. A. Kralchevsky, K. Nagayama), Elsevier Science, Oxford **2001**, pp. 469–502.
- [41] M. Varenberg, B. Murarash, Y. Kligerman, S. N. Gorb, *Appl. Phys. A* **2011**, *103*, 933.
- [42] M. Kamperman, E. Kroner, A. del Campo, R. M. McMeeking, E. Arzt, *Adv. Eng. Mater.* **2010**, *12*, 335.
- [43] H. Lee, B. P. Lee, P. B. Messersmith, *Nature* **2007**, *448*, 338.
- [44] L. Wang, Y. Hui, C. Fu, Z. Wang, M. Zhang, T. Zhang, *J. Adhes. Sci. Technol.* **2020**, *34*, 2275.
- [45] W. Ruotolo, D. Brouwer, M. R. Cutkosky, *Sci. Robot.* **2021**, *6*, eabi9773.
- [46] X. Li, D. Tao, H. Lu, P. Bai, Z. Liu, L. Ma, Y. Meng, Y. Tian, *Surf. Topogr.: Metrol. Prop.* **2019**, *7*, 023001.
- [47] T. G. Chen, A. Cauligi, S. A. Suresh, M. Pavone, M. R. Cutkosky, *IEEE Robot. Autom. Mag.* **2022**, *29*, 24.
- [48] T. T. Hoang, J. J. S. Quek, M. T. Thai, P. T. Phan, N. H. Lovell, T. N. Do, *Sens. Actuator A Phys.* **2021**, *323*, 112673.
- [49] A. Wang, S. Keten, *Npj. Comput. Mater.* **2019**, *5*, 29.
- [50] T. Doi, H. Takagi, N. Shimizu, N. Igarashi, S. Sakurai, *ACS Appl. Polym. Mater.* **2020**, *2*, 4973.
- [51] X. Deng, *J. Adhes.* **2018**, *94*, 77.
- [52] B. Sharma, A. Sandilya, U. Patel, A. Shukla, S. D. Sadhu, *Int. J. Adhes. Adhes.* **2021**, *110*, 102946.
- [53] J. Moon, Y. Huh, J. Park, H. W. Kim, Y. Choe, J. Huh, J. Bang, *ACS Appl. Polym. Mater.* **2020**, *2*, 2444.